J. Ocean Univ. China (Oceanic and Coastal Sea Research)
https://doi.org/10.1007/s11802-022-5207-8
ISSN 1672-5182, 2022 21 (6): 1529-1537
http://www.ouc.edu.cn/xbywb/
E-mail:xbywb@ouc.edu.cn

Processes Controlling the Carbonate Chemistry of Surface Seawater Along the 150°E Transect in the Northwest Pacific Ocean

MOU Liang[1)], ZHANG Honghai[2)], CHEN Zhaohui[3)], and HU Yubin[1), *]

1) *Institute of Marine Science and Technology*, *Shandong University*, *Qingdao* 266237, *China*
2) *Frontiers Science Center for Deep Ocean Multispheres and Earth System*, *and Key Laboratory of Marine Chemistry Theory and Technology*, *Ministry of Education*, *Ocean University of China*, *Qingdao* 266100, *China*
3) *Physical Oceanography Laboratory*, *Ocean University of China*, *Qingdao* 266100, *China*

(Received September 24, 2021; revised April 22, 2022; accepted May 13, 2022)
© Ocean University of China, Science Press and Springer-Verlag GmbH Germany 2022

Abstract The problem of ocean acidification caused by the increase of atmospheric carbon dioxide concentration is becoming increasingly prominent. Field observation in the northwest Pacific Ocean was carried out along the 150°E transect in November 2019. The distribution characteristics and influencing factors of the surface seawater carbonate chemistry, including dissolved inorganic carbon (DIC), total alkalinity (TA), pH, partial pressure of carbon dioxide (pCO_2) and aragonite saturation state (Ω_{arag}) were investigated. DIC and TA ranged from 1915 to 2014 μmol kg^{-1} and 2243 to 2291 μmol kg^{-1}, respectively; DIC in general decreased with decreasing latitude, but TA had no clear latitudinal gradient. pCO_2 values increased with the decrease of latitude and were all below the atmospheric pCO_2 level, ranging from 332 to 387 μatm. pH on the total hydrogen ion concentration scale (pH_T) decreased with the decrease of latitude in the range of 8.044–8.110, while Ω_{arag} increased with the decrease of latitude in the range of 2.61–3.88, suggesting that the spatial distributions of pH_T and Ω_{arag} were out of phase. Compared with the present, the predicted values of pH_T and Ω_{arag} by the end of this century would decrease remarkedly; larger declines were found in the higher pH_T and Ω_{arag} regions, resulting in the differences along the meridional gradient becoming smaller for both pH_T and Ω_{arag}.

Key words ocean acidification; carbonate system; aragonite saturation state; seawater pH; Pacific Ocean

1 Introduction

The ocean is one of the largest carbon sinks, absorbing about 30% of anthropogenic CO_2 since pre-industrial times (Sabine *et al*., 2004; Cai *et al*., 2010). However, the CO_2 absorbed by the ocean reacts with seawater, resulting in a decrease in pH (Byrne *et al*., 2010), which is called the ocean acidification (Caldeira and Wickett, 2003; Feely *et al*., 2004). The average surface pH of seawater, which was about 8.2 before the industrial revolution, has dropped by 0.1 (Orr *et al*., 2005; Feely *et al*., 2009). The pH is expected to decline by a further 0.3–0.5 units by the end of this century and global surface ocean pH would become increasingly more homogeneous with time (Brewer, 1997; Jiang *et al*., 2019). The pH can directly reflect the amount of H^+ in seawater, which is an important measure of ocean acidification. Dore *et al*. (2009) reported time-series measurements of seawater pH and related parameters at the ALOHA observatory near the central North Pacific over the past 20 years, and found a significant long-term downward trend of about -0.0019 ± 0.0002 y^{-1} in the pH of surface seawater, in response to the increase of the global atmospheric CO_2 concentration. In addition, aragonite has a higher solubility than calcite, resulting in organisms with aragonite calcium carbonate as their structure more susceptible to ocean acidification (Mucci, 1983; Fabry *et al*., 2009). Therefore, the aragonite saturation state (Ω_{arag}) is also commonly used to assess the impact of ocean acidification on calcareous organisms. The oceanic uptake of anthropogenic CO_2 would result in concomitant changes in seawater chemistry and adverse consequences for many organisms (Gattuso *et al*., 1999; Langdon and Atkinson, 2005; Iglesias-Rodriguez *et al*., 2008). Although pH and Ω_{arag} are two commonly used parameters in assessing the impact of ocean acidification, factors (*e.g*., temperature, CO_2 gas exchange) affecting the distributions of pH and Ω_{arag} could be quite different (Cai *et al*., 2020).

Previous work in the West Pacific Ocean has focused on the study of air-sea CO_2 exchange (Dore *et al*., 2003; McKinley *et al*., 2004), and the carbonate system as well as its related influence factors (Murata *et al*., 2009; Wakita *et al*., 2010). For example, Murata *et al*. (2009) studied

* Corresponding author. E-mail: yubinhu@sdu.edu.cn

the interdecadal variability of anthropogenic CO_2 along the 149˚E transect of the Northwest Pacific Ocean and Wakita *et al*. (2010) analyzed the interdecadal variation of DIC in the Northwest Pacific Ocean from 1992 to 2008. Both studies revealed the decadal variation of a single carbonate system parameter. However, the investigated data on the carbonate system are still scarce in this region. In this study, we investigated the whole carbonate chemistry of the surface seawater, including DIC, TA, pCO_2, pH and Ω_{arag} along the 150˚E transect in the Northwest Pacific Ocean. We also predicted the changes in pH and Ω_{arag} by the end of this century. This study aimed to reveal factors controlling the meridional distributions of the carbonate chemistry, with a special interest in the distributions of surface seawater pH and Ω_{arag}.

2 Materials and Methods

2.1 Study Area

The survey area (40˚–13˚N, 150˚E) is located northwest of the Pacific Ocean, whose hydrological conditions are affected by ocean currents and different water masses (Fig.1). From north to south, the survey area is affected by the Subarctic Current, Kuroshio Extension, Subtropical Countercurrent and North Equatorial Current. The Subar- ctic Current passing through the survey area is around 40˚N, which originates from the subarctic North Pacific Ocean dominated by upwelling. The Kuroshio Extension is around 34˚N, which is formed by the eastward turning of the Kuroshio Current near the Japan coast. The Subtropical Countercurrent is found in the latitudinal band of 22˚–25˚N, and the North Equatorial Current exists at the southern end of the survey area (Qiu, 2001).

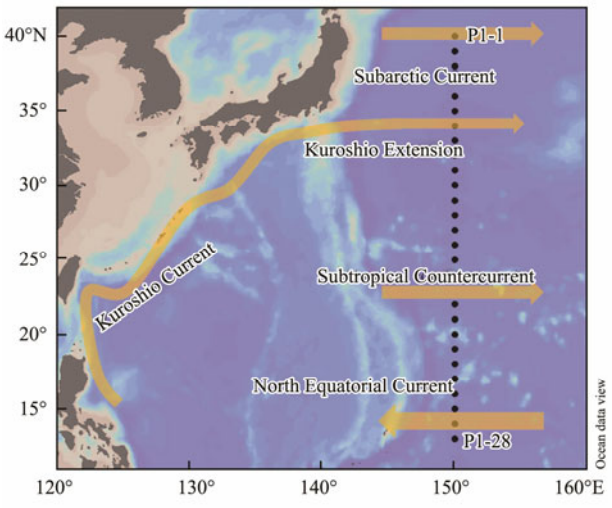

Fig.1 Sampling stations in the Northwest Pacific Ocean.

2.2 Sampling

Surface seawater samples were collected at each latitude (at an interval of 1 degree) from 40˚N to 13˚N along the 150˚E transect (P1) aboard *R/V* '*Dongfanghong 3*' in November 2019, except for stations P1-4, P1-17 and P1-18 (Fig.1). Water samples were collected using Niskin bottles mounted on a Seabird CTD system (911-plus, Seabird Corporation), which also measured the temperature and salinity of seawater. Duplicate pH samples were collected into 40 mL brown borosilicate glass vials after overflowing with at least twice their volume to minimize exposure with air. TA samples were collected into 250 mL high-density polyethylene (HDPE) bottles, immediately poisoned with 10 μL of saturated $HgCl_2$, then stored in the dark at room temperature and brought back to the land laboratory for analysis within two months.

2.3 Analytical Methods

TA was determined by Gran titration using an open-cell with an automatic potentiometric titration system (T960, Hanon), and the concentration of HCl was calibrated using seawater certified reference materials (CRMs, Batch 178) from A. G. Dickson lab. Each sample was measured three times, using aged Pacific surface seawater with known TA values for quality control, with an accuracy of 0.1%. The pH samples were measured on board on the total hydrogen ion concentration scale ($pH_{T,\,25}$) at 25 ± 0.05℃ in a thermal bath using two independent benchtop pH meters (star A211, Thermo Fisher Scientific), each equipped with a combination electrode (8157BNUMD). The pH values were calibrated against the Tris buffer (pH = 8.094 at 25℃) from A. G. Dickson lab and converted to *in situ* temperatures (referred to as pH_T hereafter) using CO2SYS v2.1 program (Pierrot *et al*., 2006), with an overall precision of ± 0.005 pH units.

Knowing any two of the four carbonate system parameters (pH, TA, DIC and pCO_2), the others of the carbonate chemistry can be calculated based on the thermodynamic properties (Millero, 2007). Thus, pH_T, DIC, pCO_2, Ω_{arag} and Revelle factor (RF) were calculated from the measured $pH_{T,\,25}$ and TA data, using CO2SYS v2.1 program (Pierrot *et al*., 2006), together with the *in situ* temperature and salinity, and with the equilibrium constants of the carbonate acid K_1 and K_2 from Mehrbach *et al*. (1973) refit by Dickson and Millero (1987), the K_{HSO4} was from (Dickson, 1990), and the $[B]_T$ value from Uppström (1974). In order to assess the quality of the calculated data, DIC of an aged Pacific surface seawater (measured by a DIC analyzer (AS-C5, Apollo SciTech)) was compared with the one calculated from the pH_T and TA values which were measured by the same protocol as mentioned above. The difference between the measured and calculated DIC was within ± 2 μmol kg^{-1}, suggesting the calculated DIC data were reliable.

2.4 Predictions of pH_T and Ω_{arag} by the End of This Century

Current predictions suggest that atmospheric pCO_2 will rise to (900 ± 50) ppm by 2100 and the rise in global mean surface temperature is likely to be 1.4℃ to 3.1℃ higher than present (IPCC RCP 6.0 projections). To predict the distributions of *in situ* surface seawater pH_T and Ω_{arag} by 2100, we assumed a CO_2 concentration of 900 ppm in the

atmosphere and a temperature 2℃ higher. We further assumed that surface ocean pCO_2 changes at the same rate as the atmospheric pCO_2 and the sea surface temperature (SST) will also rise by 2℃ by 2100 without TA changing over time. Surface seawater pH_T and Ω_{arag} at each sampling station along the P1 transect in 2100 were calculated from the surface seawater pCO_2 and TA using CO2SYS program.

2.5 Statistical Analysis

The distributions of surface seawater temperature, salinity, DIC, TA, pH_T, Ω_{arag}, pCO_2 and RF along 150°E transect from 40°N to 13°N were plotted using Ocean data view (Schlitzer, 2018). Correlation analysis in this study was performed by the Pearson correlation test using GraphPad Prism 8, with a significance level of 99%.

3 Results

3.1 Hydrographic Conditions

SST was in the range of 14.5–29.4℃ with a mean value of 26.0℃ and exhibited a clear latitudinal distribution (Fig.2a), increasing with decreasing latitude with abnormally low values at two northernmost stations (40°N and 39°N). The salinity was in the range of 33.46–35.04, with a mean value of 34.56, and the lowest values were also found at the two northernmost stations (Fig.2b), which were 33.61 and 33.46, respectively. Except for those two northernmost stations, the salinity of the rest stations was above 34 and generally followed bimodal distribution. The distributions of SST and salinity along the P1 transect revealed that the two northernmost stations were

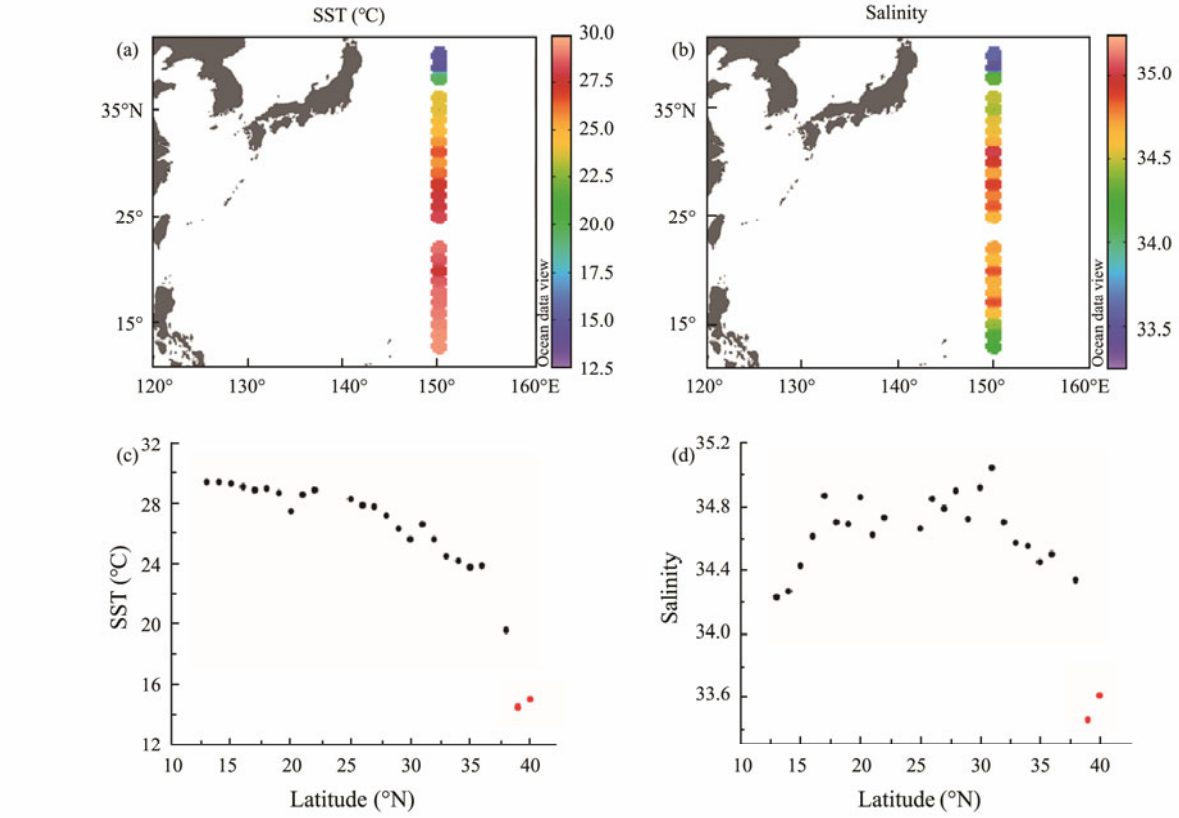

Fig.2 Distributions of sea surface temperature (a), salinity (b) and variations of sea surface temperature (c) and salinity (d) with latitude along 150°E transect.

likely under the impact of the Subarctic Current, which is low in temperature and salinity.

3.2 Distributions of Carbonate Chemistry

DIC values ranged from 1915 to 2014 μmol kg^{-1}, decreasing with the decrease of latitude, with a mean value of 1954 μmol kg^{-1} (Fig.3a). TA was in the range of 2243 – 2291 μmol kg^{-1}, with a mean value of 2270 μmol kg^{-1}; it increased gradually from 40°N to 31°N and high values appeared near 31°N. South of 31°N, there was no latitudinal gradient in TA distribution (Fig.3b). The salinity-normalized DIC and TA (nDIC = DIC/S*35, nTA = TA/S*35) ranged from 1949 to 2107 μmol kg^{-1} and 2288 to 2352 μmol kg^{-1} along the P1 transect, respectively, with abnormally high values both at the two northernmost stations (Figs.3c and d). In general, nDIC decreased with decreasing latitude. But for nTA, except for the two northernmost stations, nTA of other stations were obviously lower and relatively homogeneous. The surface seawater pH_T ranged from 8.044 to 8.110, displaying a clear decrease pattern from north to south along the P1 transect (Fig.3e). Ω_{arag} also exhibited a significantly latitudinal pattern, but in contrast to pH_T, it increased with decreasing latitude, ranging from 2.61 to 3.88 (Fig.3f). The surface seawater pCO_2 was in the range of 332–387 μatm, increasing with the decrease of latitude (Fig.3g); all of them were well below the atmospheric pCO_2 which was around 412 μatm during the survey period (Dlugo-

kencky and Tans, 2019), indicating that the whole survey area was a CO_2 sink. The difference in pCO_2 between the atmosphere and surface seawater ($\Delta pCO_2 = pCO_{2,\,air} - pCO_{2,\,seawater}$) decreased from north to south, ranging from 80 to 25 μatm, indicating that the northern area was a stronger CO_2 sink. The spatial distribution of RF showed a clear meridional gradient along the P1 transect (Fig.3h), decreasing with the decrease of latitude from 11.02 to 8.98, with abnormally high values at the two northernmost stations.

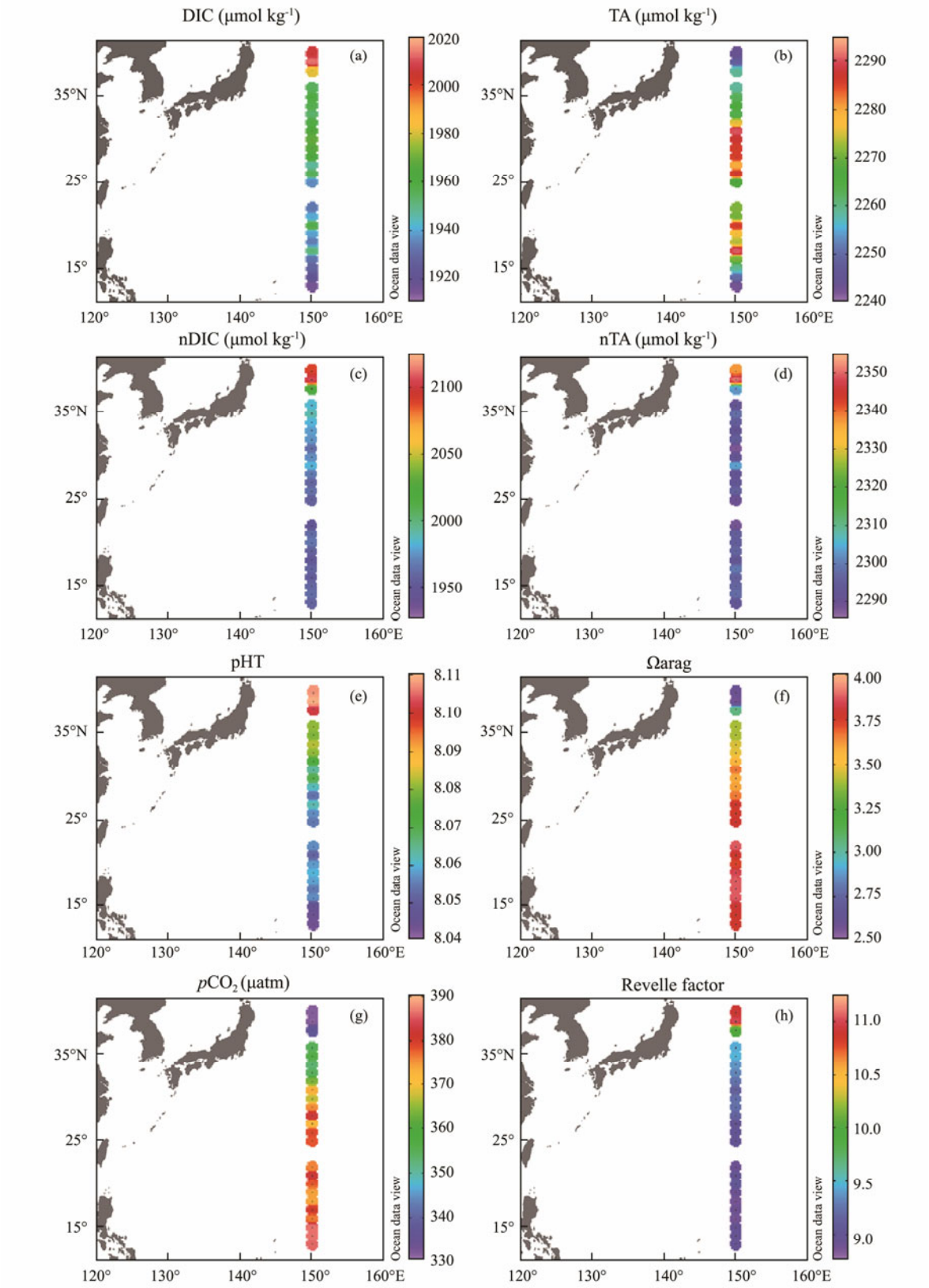

Fig.3 Distributions of carbonate chemistry along 150˚E transect. (a), DIC; (b), TA; (c), nDIC; (d), nTA; (e), pH_T; (f), Ω_{arag}; (g), pCO_2; and (h), Revelle factor.

4 Discussion

4.1 Factors Affecting the Distributions of DIC, TA, pCO_2 and RF

In order to better understand the processes controlling the distributions of carbonate chemistry, the survey regions along the P1 transect were divided into two subregions, namely, region 1 (stations from 38° to 13°N) and region 2 (the Subarctic Current dominant regions: stations 40° and 39°N), according to the SST-latitude and salinity-latitude diagrams (Figs.2c and d).

In region 1, DIC decreased from north to south along the P1 transect, while no clear pattern was found for TA. The variation of TA was closely related to salinity change ($r = 0.96$, $P < 0.0001$) (Fig.4a), indicating that TA was mainly controlled by water mixing. In regard to DIC, it is not only affected by the salinity change but also greatly affected by the air-sea CO_2 exchange and biological activities (Cai *et al.*, 2020). In this study, there was a certain correlation between DIC and ΔpCO_2 ($r=0.63$, $P=0.0012$) (Fig.4b). Since surface seawater pCO_2 values along the P1 transect were all below the atmospheric pCO_2 level, the larger ΔpCO_2 leads to more CO_2 being absorbed, resulting in higher DIC values in the northern parts of P1 transect. The Subarctic Current that originates from the subarctic North Pacific Ocean dominated by upwelling causes surface water around region 2 to have abnormally high TA and DIC, compared to the values predicted by the regression lines from region 1 (red dots in Figs.4a and b).

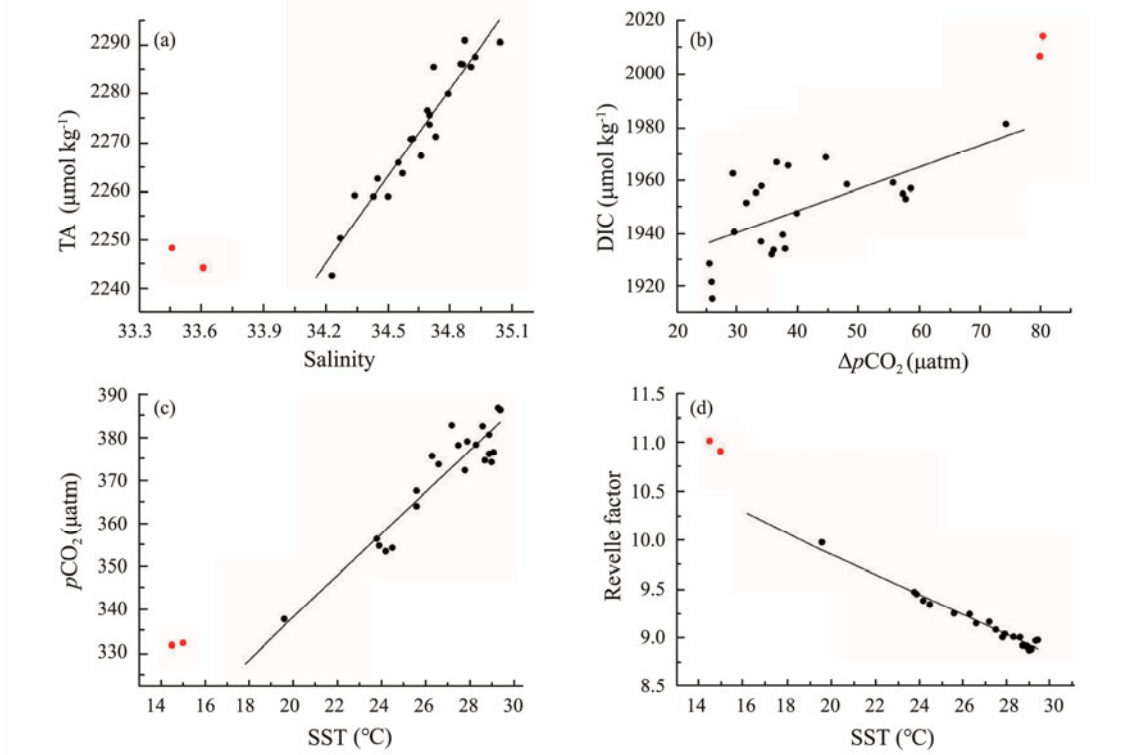

Fig.4 Relationships between TA and salinity (a), DIC and ΔpCO_2 (b), pCO_2 and sea surface temperature (c), Revelle factor and sea surface temperature (d). Red dots represent stations 40° and 39°N of the 150°E transect.

The strong positive correlation between temperature and pCO_2 ($r=0.93$, $P<0.0001$, excluding the two northmost stations) (Fig.4c) indicated that temperature plays an important role in latitudinal surface seawater pCO_2 distribution. The higher the temperature, the lower the solubility of CO_2, which results in an increase in seawater pCO_2 and a decrease in carbon sink intensity. The pCO_2 values of the two northernmost stations (red dots in Fig.4c) were significantly higher than those predicted by the regression line from region 1, possibly due to the impact of the Subarctic Current. Nevertheless, the surface seawater pCO_2 remained substantially lower than the atmospheric pCO_2, reflecting the important role of low SST in keeping pCO_2 low *via* thermodynamic equilibrium shift and in maintaining a significant air-sea CO_2 disequilibrium (Cai *et al.*, 2020).

RF, defined as the ratio between the fractional change in pCO_2 to the fractional change in DIC under the condition of constant temperature, salinity and TA, is a measure of the buffering capacity of seawater (Zeebe and Wolf-Gladrow, 2001). RF can be regarded as a function of temperature, which decreased with increasing temperature ($r=-0.98$, $P<0.0001$, excluding the two northmost stations) (Fig.4d), explaining the latitudinal variation of RF along the P1 transect from north to south. The abnormally high RF values (red dots in Fig.4d) at the northern ends of P1 are mainly related to the abnormally low salinity and TA caused by the Subarctic Current passing through this region.

4.2 Effects of SST and ΔpCO_2 on pH and Ω_{arag}

From the north (40°N) to the south (13°N) along the P1

transect, the SST increased by nearly 15℃ and ΔpCO_2 decreased by 54 μatm, which provides a favorable condition for studying the effects of spatial variations of temperature and ΔpCO_2 on pH and Ω_{arag}. The spatial variations of pH_T and Ω_{arag} between the northern end (40°N) and the southern end (13°N) along the P1 transect were 0.064 and −1.20, respectively. There were strong correlations between pH_T and SST (Fig.5a, $r=-0.96$, $P<0.0001$), and between Ω_{arag} and SST (Fig.5b, $r=0.99$, $P<0.0001$), indicating that SST might play important roles in spatial distributions of pH_T and Ω_{arag}. According to Jiang *et al.* (2019) and Xue *et al.* (2020), the influence of temperature on pH and Ω_{arag} can be divided into two aspects, namely, the internal temperature effect and the external temperature effect. The internal temperature effect refers to changing the existing form of CO_2 dissolved in water under constant TA and DIC conditions (*i.e.*, closed system), increasing the dissociation of HCO_3^- and H_2O and the concentration of H^+ and CO_3^{2-}, thus decreasing pH and increasing Ω_{arag}. The external temperature effect refers to the gas exchange caused by the change in CO_2 solubility, which decreases with increasing temperature, resulting in a decrease in seawater CO_2 concentration, thus increasing both pH and Ω_{arag}. By altering the acid-base equilibrium of the carbonate system and CO_2 solubility-driven air-sea exchange, the combined effects of temperature would cancel out for pH resulting in little change of pH with temperature, whereas they reinforce each other for Ω_{arag}. However, this hypothesis might not be completely true when air-sea CO_2 disequilibrium or other nonthermal components (*e.g.*, water mass mixing and biological processes) have to be taken into consideration. As revealed by the study of Xue *et al.* (2021), if the seawater is under air-sea disequilibrium or under the influences of water mass mixing or biological processes, pH would be either more controlled by the thermal or nonthermal components, depending on their competing effects, while Ω_{arag} would be almost always dominated by its nonthermal components. In this study, pH_T decreased with the increasing temperature, suggesting that it is more controlled by the thermal components (*i.e.*, internal temperature effect, Fig.5a, red dashed line) than the nonthermal components. However, the effect of the thermal components on pH was about 0.21, but the actual pH_T decreased only about 0.06, indicating that the effect of the thermal components was partially counteracted by the nonthermal processes. Although Ω_{arag} was positively correlated with SST, the thermal components only partially contribute to an increase in Ω_{arag} (Fig.5b, red dashed line).

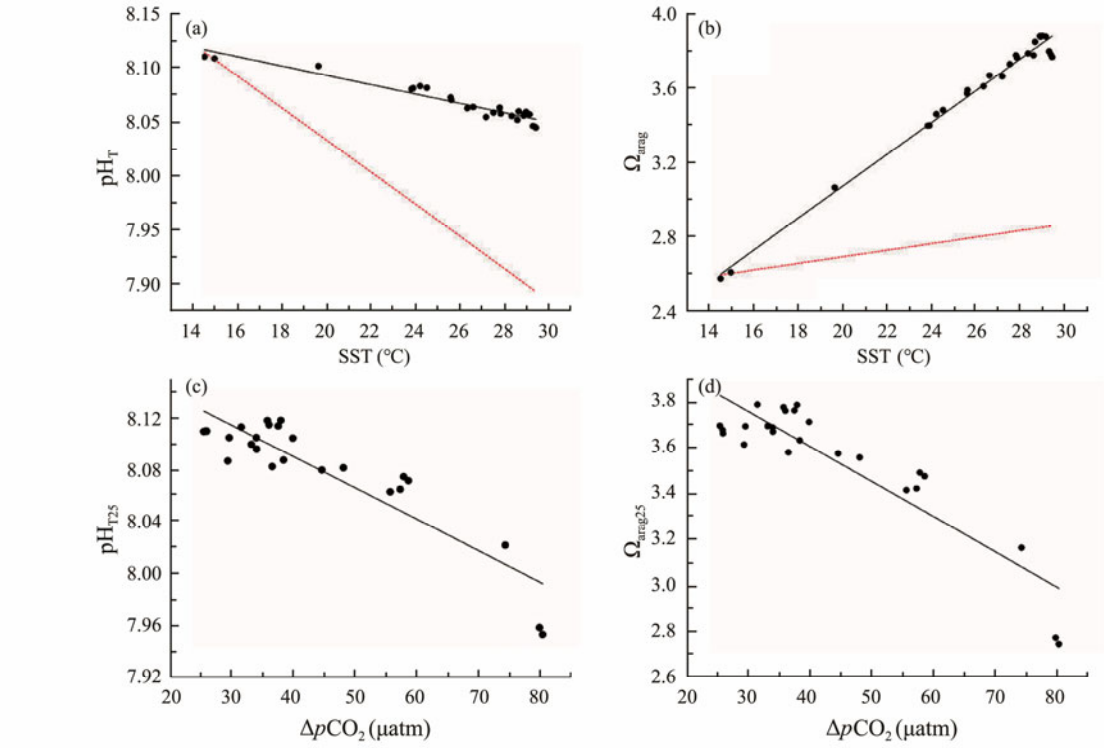

Fig.5 Relationships between pH_T and sea surface temperature (a), Ω_{arag} and sea surface temperature (b), $pH_{T,25}$ and ΔpCO_2 (c), $\Omega_{arag,25}$ and ΔpCO_2 (d). Red dashed line in (a) and (b) represents the internal temperature effect (calculated at constant S =33.61, TA = 2244 μmol kg^{-1} and DIC = 2207 μmol kg^{-1}, based on the data from P1-1 station).

To further understand the impact of the nonthermal components on pH and Ω_{arag}, we examined the correlations of ΔpCO_2 ($\Delta pCO_2 = pCO_{2,\,air} - pCO_{2,\,seawater}$, and $\Delta pCO_2 > 0$ along the investigated P1 transect) with pH and Ω_{arag}, which were normalized to the temperature of 25℃ ($pH_{T,\,25}$ and $\Omega_{arag,\,25}$) to remove the thermal components. As shown in Figs.5c and d, both $pH_{T,\,25}$ and $\Omega_{arag,\,25}$ are negatively correlated with ΔpCO_2 ($r=-0.90$, $P<0.0001$ and $r=-0.96$, $P<0.0001$, respectively), which is due to the fact that ΔpCO_2 to a large extent represents the nonthermal components, while the nonthermal components of both pH and omega are in phase; larger ΔpCO_2

would result in more CO_2 being absorbed, which would reduce the pH and Ω_{arag} in the same direction (Xue *et al*., 2021). Thus, from north to south along the P1 transect, although a decrease in ΔpCO_2 would increase pH, the effect is outweighed by the impact of temperature increase, resulting in a decrease in pH_T from high latitude to low latitude, while both an increase in temperature and a decrease in ΔpCO_2 (main controlling factor) increase the Ω_{arag}.

4.3 pH and Ω_{arag} by the End of This Century

The spatial distribution characteristics of pH_T and Ω_{arag} along the P1 transect at the end of this century under the IPCC RCP 6.0 projection were similar to the present (Figs.6a and b). pH_T^{2100} was in the range of 7.769−7.748, slightly decreasing with the decrease of latitude. Ω_{arag}^{2100} increased with decreasing latitude, ranging from 1.40 to 2.40. Both pH_T and Ω_{arag} showed large declines compared with the present (Figs.6c and d). The declines in pH_T and Ω_{arag} ranged from −0.343 to −0.296 and −1.17 to −1.50, respectively, in response to the temperature rise and the accumulation of atmospheric CO_2 concentration as projected. The decline in pH is consistent with the modeling study by Jiang *et al*. (2019), showing that the global average surface seawater pH_T decreased by about 0.33 ± 0.04 units from 2000 to 2100 under the RCP8.5 'business-as-usual' scenario. As discussed above, two effects of temperature mainly cancel out for pH, whereas they reinforce each other for Ω_{arag} (*i.e*., Ω_{arag} would increase with temperature increase). Therefore, the rise of temperature by the end of this century contributes little to the decline in pH and Ω_{arag}, but rather the accumulation of the atmospheric CO_2, which leads to a continuous increase in atmospheric pCO_2, forcing more atmospheric CO_2 into seawater through the sea-air exchange, resulting in an increase in H^+ and a decrease in CO_3^{2-}, thus leading to the decrease of both pH and Ω_{arag}.

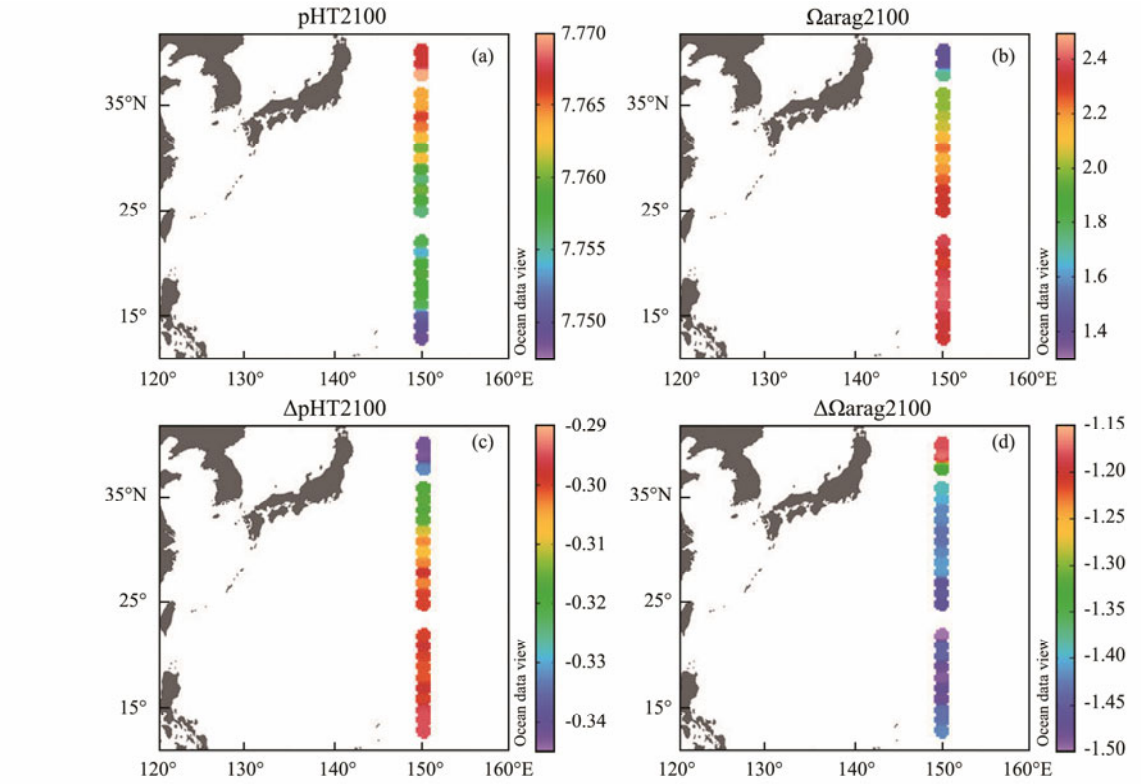

Fig.6 Distributions of pH_T (a), Ω_{arag} (b) along 150˚E transect at the end of this century and the decline in pH_T (ΔpH_T) (c) and Ω_{arag} ($\Delta\Omega_{arag}$) (d) from the present to the year of 2100 ΔpH_T.

The decline in pH_T from the present to the year of 2100 (ΔpH_T) decreased with decreasing latitude; ΔpH_T was larger at high latitudes than that at low latitudes along the P1 transect (Fig.6c), which is closely related to the distribution of RF. RF is a good indicator of ocean buffer capacity; the higher its value is, the weaker the buffer capacity of seawater will be, and the greater the pH change will be, resulting in a smaller latitudinal difference in pH along the P1 transect. The decline in pH_T is consistent with the result obtained by Jiang *et al*. (2019) that the pH of global ocean surface water would gradually become homogenous with time. The decline in Ω_{arag} from the present to the year of 2100 showed a different latitudinal distribution pattern, which was slow in the northern end stations (*i.e*., the Subarctic Current dominant region), and relatively uniform and fast at low latitudes (Fig.6d). This is consistent with the findings of Feely *et al*. (2018) that the decreasing rate of Ω_{arag} is faster in warm and high Ω_{arag} waters. In a word, the decline in pH and Ω_{arag} over time can vary differently in cold high latitude *vs*. warm low latitude waters, which is consistent with the findings from the American ocean margins (Cai *et al*., 2020).

5 Conclusions

The distribution patterns of carbonate chemistry along the 150˚E from 40˚N to 13˚N and their controlling factors were investigated in November 2019. The Subarctic Current at the northern ends caused abnormally low temperatures and salinities of the surface seawater, and high values of nDIC and nTA. DIC and Revell factor decreased with the decrease of latitude, while pCO_2 increased with the decrease of latitude but all were below atmospheric pCO_2 level, resulting in a decrease in ΔpCO_2 from north to south. The distributions of pH_T and Ω_{arag} were out of phase; from north to south, pH_T was more controlled by the thermal components resulting in a decrease in pH_T while the increase of temperature and the decrease of ΔpCO_2 both increased the Ω_{arag}. In addition, pH_T and Ω_{arag} along 150˚E at the end of this century were predicted to decrease but at different decline rates, with larger declines in higher pH_T and Ω_{arag} regions, suggesting that meridional gradients of pH_T and Ω_{arag} would become homogenous with time in future.

Acknowledgements

This study was supported by the Key Research and Development Program of Shandong Province (No. 2020 ZLYS04), the National Key Research and Development Program of China (No. 2017YFA0604300), the Qingdao Pilot National Laboratory for Marine Science and Technology (No. 2018SDKJ0105-1), the Fundamental Research Funds for the Central Universities (No. 202072 001), and the Young Scholars Program of Shandong University (No. 2018WLJH43). We wish to thank crew members of the *R/V* '*Dongfanghong 3*' for their help during the investigation.

References

Brewer, P. G., 1997. Ocean chemistry of the fossil fuel CO_2 signal: The haline signal of 'business as usual'. *Geophysical Research Letters*, **24** (11): 1367-1369, DOI: 10.1029/97gl01179.

Byrne, R. H., Mecking, S., Feely, R. A., and Liu, X., 2010. Direct observations of basin-wide acidification of the North Pacific Ocean. *Geophysical Research Letters*, **37**: L02601, DOI: 10.1029/2009gl040999.

Cai, W. J., Hu, X., Huang, W. J., Jiang, L. Q., Wang, Y., Peng, T. H., *et al*., 2010. Alkalinity distribution in the western North Atlantic Ocean margins. *Journal of Geophysical Research: Oceans*, **115**: C08014, DOI: 10.1029/2009jc005482.

Cai, W. J., Xu, Y. Y., Feely, R. A., Wanninkhof, R., Jonsson, B., Alin, S. R., *et al*., 2020. Controls on surface water carbonate chemistry along North American ocean margins. *Nature Communications*, **11** (1): 2691, DOI: 10.1038/s41467-020-16530-z.

Caldeira, K., and Wickett, M. E., 2003. Anthropogenic carbon and ocean pH. *Nature*, **425** (6956): 365-365, DOI: 10.1038/425365a.

Dickson, A. G., 1990. Standard potential of the reaction: AgCl(s) + $1/2H_2$(g) = Ag(s) + HCl(aq), and the standard acidity constant of the ion HSO_4^- in synthetic sea water from 273.15 to 318.15 K. *Journal of Chemical Thermodynamics*, **22** (2): 113-127, DOI: 10.1007/978-1-61779-117-8_26.

Dickson, A. G., and Millero, F. J., 1987. A comparison of the equilibrium constants for the dissociation of carbonic acid in seawater media. *Deep-Sea Research*, **34** (10): 1733-1743, DOI: 10.1016/0198-0149(87)90021-5.

Dlugokencky, E., and Tans, P., 2019. Trends in atmospheric carbon dioxide, National Oceanic and Atmospheric Administration, Earth System Research Laboratory (NOAA/ESRL), http://www.esrl.noaa.gov/gmd/ccgg/trends/global. html.

Dore, J. E., Lukas, R., Sadler, D. W., and Karl, D. M., 2003. Climate-driven changes to the atmospheric CO_2 sink in the subtropical North Pacific Ocean. *Nature*, **424** (6950): 754-757, DOI: 10.1038/nature01885.

Dore, J. E., Lukas, R., Sadler, D. W., Church, M. J., and Karl, D. M., 2009. Physical and biogeochemical modulation of ocean acidification in the central North Pacific. *PNAS*, **106** (30): 12235-12240, DOI: 10.1073/pnas.0906044106.

Fabry, V. J., McClintock, J. B., Mathis, J. T., and Grebmeier, J. M., 2009. Ocean acidification at high latitudes: The Bellweather. *Oceanography*, **22** (4): 160-171, DOI: 10.5670/oceanog.2009.105.

Feely, R. A., Doney, S. C., and Cooley, S. R., 2009. Ocean acidification: Present conditions and future changes in a high-CO_2 world. *Oceanography*, **22** (4): 36-47, DOI: 10.5670/oceanog.2009.95.

Feely, R. A., Okazaki, R. R., Cai, W. J., Bednarsek, N., Alin, S. R., Byrne, R. H., *et al*., 2018. The combined effects of acidification and hypoxia on pH and aragonite saturation in the coastal waters of the California current ecosystem and the northern Gulf of Mexico. *Continental Shelf Research*, **152**: 50-60, DOI: 10.1016/j.csr.2017.11.002.

Feely, R. A., Sabine, C. L., Lee, K., Berelson, W., Kleypas, J., Fabry, V. J., *et al*., 2004. Impact of anthropogenic CO_2 on the $CaCO_3$ system in the oceans. *Science*, **305** (5682): 362-366, DOI: 10.1126/science.1097329.

Gattuso, J. P., Allemand, D., and Frankignoulle, M., 1999. Photosynthesis and calcification at cellular, organismal and community levels in coral reefs: A review on interactions and control by carbonate chemistry. *American Zoologist*, **39** (1): 160-183.

Iglesias-Rodriguez, M. D., Halloran, P. R., Rickaby, R. E., Hall, I. R., Colmenero-Hidalgo, E., Gittins, J. R., *et al*., 2008. Phytoplankton calcification in a high-CO_2 world. *Science*, **320** (5874): 336-340, DOI: 10.1126/science.1154122.

Jiang, L. Q., Carter, B. R., and Feely, R. A., 2019. Surface ocean pH and buffer capacity: Past, present and future. *Scientific Reports*, **9**: 18624, DOI: 10.1038/s41598-019-55039-4.

Langdon, C., and Atkinson, M. J., 2005. Effect of elevated pCO_2 on photosynthesis and calcification of corals and interactions with seasonal change in temperature/irradiance and nutrient enrichment. *Journal of Geophysical Research: Oceans*, **110** (C9): C09S07, DOI: 10.1029/2004jc002576.

McKinley, G. A., Rodenbeck, C., Gloor, M., Houweling, S., and Heimann, M., 2004. Pacific dominance to global air-sea CO_2 flux variability: A novel atmospheric inversion agrees with ocean models. *Geophysical Research Letters*, **31** (22): L22308, DOI: 10.1029/2004gl021069.

Mehrbach, C., Culberson, C. H., Hawley, J. E., and Pytkowicz, R. M., 1973. Measurement of the apparent dissociation constants of carbonic acid in seawater at atmospheric pressure. *Limnology and Oceanography*, **18** (6): 897-907, DOI: 10.

4319/lo.1973.18.6.0897.

Millero, F. J., 2007. The marine inorganic carbon cycle. *Chemical Reviews*, **107** (2): 308-341, DOI: 10.1021/cr0503557.

Mucci, A., 1983. The solubility of calcite and aragonite in seawater at various salinities, temperatures, and one atmosphere total pressure. *American Journal of Science*, **283** (7): 780-799, DOI: 10.2475/ajs.283.7.780.

Murata, A., Kumamoto, Y., Sasaki, K. I., Watanabe, S., and Fukasawa, M., 2009. Decadal increases of anthropogenic CO_2 along 149˚E in the western North Pacific. *Journal of Geophysical Research: Oceans*, **114** (4): C04018.

Orr, J. C., Fabry, V. J., Aumont, O., Bopp, L., Doney, S. C., Feely, R. A., *et al*., 2005. Anthropogenic ocean acidification over the twenty-first century and its impact on calcifying organisms. *Nature*, **437** (7059): 681-686, DOI: 10.1038/nature 04095.

Pierrot, D., Lewis, E., and Wallace, D. W. R., 2006. MS Excel program developed for CO_2 system calculations. ORNL/CDIAC-105a. Carbon dioxide information analysis center, Oak Ridge National Laboratory, U.S. Department of energy, Oak Ridge, Tennessee. DOI: 10.3334/CDIAC/otg.CO2SYS_ XLS_CDI AC105a.

Qiu, B., 2001. *Kuroshio and Oyashio Currents*. Aca- demic Press, San Diego, 1413-1425.

Sabine, C. L., Feely, R. A., Gruber, N., Key, R. M., Lee, K., Bullister, J. L., *et al*., 2004. The oceanic sink for anthropogenic CO_2. *Science*, **305** (5682): 367-371, DOI: 10.1126/science.1097403.

Schlitzer, R., 2018. Ocean Data View. https://odv.awi.de.

Uppström, L. R., 1974. Boron/chlorinity ratio of deep-sea water from Pacific Ocean. *Deep-Sea Research*, **21** (2): 161-162, DOI: 10.1016/0011-7471(74)90074-6.

Wakita, M., Watanabe, S., Murata, A., Tsurushima, N., and Honda, M., 2010. Decadal change of dissolved inorganic carbon in the subarctic western North Pacific Ocean. *Tellus B*, **62** (5): 608-620.

Xue, L., Cai, W. J., Jiang, L. Q., and Wei, Q., 2021. Why are surface ocean pH and $CaCO_3$ saturation state often out of phase in spatial patterns and seasonal cycles? *Global Biogeochemical Cycles*, **35** (7): e2021GB006949, DOI: 10.1029/2021gb006949.

Xue, L., Yang, X., Li, Y., Li, L., Jiang, L. Q., Xin, M., *et al*., 2020. Processes controlling sea surface pH and aragonite saturation state in a large northern temperate bay: Contrasting temperature effects. *Journal of Geophysical Research: Biogeosciences*, **125** (7): e2020JG005805, DOI: 10.1029/2020jg 005805.

Zeebe, R. E., and Wolf-Gladrow, D., 2001. *CO_2 in Seawater: Equilibrium, Kinetics, Isotopes, Elsevier Oceanography Series*. 65. Elsevier, Amsterdam, 346pp.

(Edited by Ji Dechun)